Surface & Coatings Technology 357 (2019) 939–946

Contents lists available at ScienceDirect

Surface & Coatings Technology

journal homepage: www.elsevier.com/locate/surfcoat

The influence of deposition parameters on the stress evolution of sputter deposited copper

Tyler Kaub[a], Zhaoxia Rao[b], Eric Chason[b], Gregory B. Thompson[a,*]

[a] University of Alabama, Department of Metallurgical & Materials Engineering, Tuscaloosa, AL 35401, United States of America
[b] Brown University, School of Engineering, Providence, RI 02912, United States of America

ARTICLE INFO

Keywords:
Thin film
Intrinsic stress
Sputter deposition
Microstructure

ABSTRACT

The growth rate and pressure dependence on the intrinsic stress in sputter deposited Cu thin films has been investigated and compared to a kinetic growth model, which contains both growth and energetic contributions to stress in its description. Since microstructure also has a strong effect on intrinsic growth stress, we have been able to systematically control a fixed grain size over multiple growth conditions spanning 0.012 nm/s to 2.4 nm/s deposition rates and 0.267 Pa to 2.667 Pa pressures using a seed layer prior to film deposition. At high deposition pressures, the stress became more tensile as the growth rate increased. In the low deposition pressure regime, the stress became more tensile with increases in deposition rate until a critical cross-over point where upon further increases in deposition rate resulted in the stress becoming more compressive. This cross-over has been explained in terms of the energetic contributions to the stress and the intrinsic high mobility of Cu to reveal this behavior. The fitting parameters and corresponding stress contributions from the kinetic model were extracted and compared to other films and deposition techniques. Though caution should be used in comparing absolute values, the kinetic model revealed the correct trends in predicting energetic trapping of defects between low and high mobility films as well as similar growth stress values, which are independent of energetic contributions, between sputtering and electrodeposition. These results suggest that the kinetic model shows promise in fitting different materials and deposition techniques intrinsic stress behavior.

1. Introduction

Thin film deposition often results in large intrinsic stresses arising from the growth process across all deposition techniques [1]. These stresses can have a significant impact on thin film performance and reliability and in some cases even alter physical properties [2]. The presence of either tensile or compressive stress can result in film failures or reduced performance through delamination, cracking and/or buckling of the film [3,4]. While research in this area has been active for well over 100 years [5], the advent of in-situ stress measurement techniques coupled with post-deposition microstructural characterization has led to the development of a fundamental understanding of the mechanisms behind intrinsic stress evolution. These studies have found a strong correlation between stress and microstructure [6–9] with tensile stresses generally associated with columnar, fine grained microstructures that are commonly observed in low atomic mobility films (denoted as Type 1 by Abermann [10]), while compressive stresses are associated with denser, high atomic mobility (Type 2) films [10].

When polycrystalline metallic thin films are deposited, depending on the growth kinetics the films may exhibit pronounced 3D growth [11] with an accompanying complex multi-stage stress evolution. If the deposited film consists of high mobility adatoms, a compressive-tensile-compressive stress evolution is observed. In contrast, low mobility adatom films exhibit a primary tensile stress evolution behavior. The initial compressive stress in both cases is believed to originate from island nucleation on the substrate surface which is attributed to Laplace pressures that lead to smaller than equilibrium lattice spacing values, which generate the initial compressive stress [12]. As the film thickens, a tensile stress will then arise from the islands on the substrate surface elastically straining to coalesce into a continuous film by forming grain boundaries with neighboring islands to reduce their surface area [13,14]. Low mobility metals will continue to exhibit this tensile stress as the film thickens through continued grain boundary formation and the associated tensile straining mechanism. For high mobility metals, a secondary post-coalescence compressive stress will occur after tensile growth whose origins have several proposed mechanisms. These include pre-coalescence compressive stress inheritance [12], capillary effects [15], excess adatoms generating stress on the surface [16], and

* Corresponding author.
E-mail address: gthompson@eng.ua.edu (G.B. Thompson).

https://doi.org/10.1016/j.surfcoat.2018.10.059
Received 12 May 2018; Received in revised form 19 October 2018; Accepted 22 October 2018
Available online 27 October 2018

insertion of excess adatoms onto film ledges [17] or into grain boundaries [18]. The understanding of this stress evolution is further compounded by the wide number of deposition techniques used to produce thin films. Techniques with high-energy particles such as sputtering, ion-beam assisted deposition and pulsed laser deposition can result in stress modification from energetic bombardments contributions (referred to as ion peening) during film growth. This can promote atomic rearrangements, dislocation generation, and/or grain boundary densification [19,20]. Such mechanisms often result in low mobility films exhibiting compressive stresses under high-energy deposition conditions. Low energy techniques, such as electrodeposition and evaporation, do not have these energetic contributions and the stress is primarily linked to growth and intrinsic material properties such as diffusivity.

To alter the intrinsic stress behavior, the deposition parameters of temperature [21], rate [22], and pressure [23] are typically adjusted. From these variations, several general trends have emerged. As the deposition temperature is increased, the mobility of the deposited atoms also increases. For low mobility films, this can result in a transition from tensile to compressive growth [21]. In higher mobility films, increases in temperature, which trigger grain growth during deposition, lead to transitions from compressive to tensile stresses [6]. With changes in growth rates, a higher deposition rate for a low mobility film will increase the tensile stress whereas a lower deposition rate for a high mobility film will lead to even larger compressive stresses [22]. As one increases the deposition pressure, the mean free path of the deposition species is decreased. For energetic based deposition techniques, reducing the arrival energy results in a reduction in the associated energetic stress generating mechanism's contribution to the film's stress state. This results in the film shifting towards a tensile stress with increasing pressure.

Clearly, a range of different stress states can form as a function of materials type and how it is deposited. This explains the variations in stresses that have been reported. For example, sputtered Mo can be highly compressive, ≈ -2.4 GPa, to highly tensile, $\approx +3.5$ GPa [24]. Similarly, electrodeposited Ni has a reported range of stresses from ≈ -60 MPa to $\approx +400$ MPa [25]. In order to relate this type of film stress variation as a function of processing conditions, a kinetic model has been proposed [26,27]. The model bases its stress generation by the events occurring at the grain boundaries as the film grows. To date, there has only been one self-contained study of different process variables (for energetic deposition) that has yielded a sufficient database that can be collectively compared to this model. This was done for a low mobility Mo film [27]. Here, this approach is expanded to a higher mobility film, Cu, over a much wider parametric range of experimental data points to test the kinetic model.

2. Kinetic model of thin film stress evolution

The equations of the model, which will be described in further detail below, are divided into two parts - a term for the stress from the film growth and two terms associated with stress effects from energetic growth mechanisms, which are additive. The model equations depend upon the kinetic parameters of growth including the effective diffusivity (D), growth rate (R), and grain size (L) with the deposition pressure (P) effects associated with the energetic contributions.

We will first consider the tensile contributing mechanism in the kinetic model. This mechanism, originally proposed by Hoffman [13], is based on the concept that the surface energy of two adjacent islands will be lowered through the creation of a grain boundary. If this event occurs, this new grain boundary reduces the free surface area of each individual island at the expense of the elastic strain necessary to close the spatial gap between the two islands. As long as the reduction in interfacial energy is larger than the strain energy, coalescence will occur. Thus, tensile stress generation will have a $1/L^{1/2}$ dependence, where L is the grain size. This relationship then predicts larger tensile stresses with smaller grain sizes because of the increased interfacial area, which has been noted experimentally [14,28]. Building upon this idea, the kinetic model by Chason [26,27] suggested that the gap closing between these islands would occur through a layer-by-layer coalescence process rather than a simultaneous closing of the gap as proposed by Hoffman.

In order to account for the compressive stress generation during growth, Chason suggested that excess adatoms could be inserting themselves into the grain boundaries [18]. This insertion is driven by a super saturation of adatoms on the surface created by the deposition flux. This flux would increase the chemical potential on the surface that would then drive the adatoms into the grain boundaries creating a compressive stress mechanisms. Upon ceasing deposition, the adatoms would then migrate out from the boundaries resulting in a stress relaxation, which is what is experimentally observed [29].

Using these two mechanisms, the total stress in the film (during non-energetic growth) can be accounted for as the balance between each mechanism, if the films are fully coalesced. This is described as

$$\sigma_{growth} = \sigma_C + (\sigma_T - \sigma_C)e^{-\frac{\beta D}{RL}} \tag{1}$$

where σ_T and σ_C are the tensile and compressive stresses respectively. The exponent term captures the growth rate, R, the grain size, L, the effective diffusivity of atoms, D, from the surface into the grain boundary, and a parameter, β, depending on the concentration of mobile defects and mechanical properties of the layer. Thus, changing R, L, and D can result in a shift in the observed stress state of the film. For example, when $\frac{\beta D}{RL} \ll 1$ the incremental stress is tensile because there is little time for excess adatoms to diffuse into the grain boundaries, whereas for the opposite conditions, $\frac{\beta D}{RL} \gg 1$, a compressive incremental stress results because the adatoms have sufficient time to diffuse into the grain boundaries.

This equation has been shown to be successful in describing non-energetic growth such as evaporation and electrodeposition [7,30]. However, for energetic deposition, like sputtering, this equation requires modification to account for collision-induced densification, or peening, of the film near the grain boundaries and the incorporation of microstructural defects into the bulk of the film. For collision-induced densification at the grain boundaries, which creates a compressive stress, the kinetic model assumes a relative range, l, for this effect. When an energetic particle hits within this range, it will introduce a compressive stress in the top most layer of the film which will be relative to the particle's energy [27]. This compressive stress originates when the atoms are incorporated into favorable sites through ballistically induced defects [31]. The stress then depends on the number of defects created per deposited atom given as

$$\sigma_{gb}^{energetic} = A_0 \times \left(\frac{l}{L}\right) \tag{2}$$

where A_0 is, an adjustable parameter used to compare the model to experimental data and will depend on the energy (pressure), growth rate, and flux of the energetic species. In this work the ratio of the flux, f, to rate, R, is assumed to be constant so that the energetic flux scales with the R allowing for one A_0 to be used in fitting the data. The $\frac{l}{L}$ term will be used to approximate the fraction of energetic particles that induce a stress in the grain boundary region and is only expected to hold true when $L > l$, which will be the case for this work.

The second energetic stress generation mechanism is linked to bulk defect incorporation where the stress from point defects is assumed to be proportional to the number of defects that are trapped in the bulk during energetic deposition. This is described as

$$\sigma_{bulk}^{energetic} = \left(1 - \frac{l}{L}\right)\sigma_0 C_{ss} \tag{3}$$

where σ_0 is the stress due to a single defect, $\left(1 - \frac{l}{L}\right)$ accounts for just the bulk of the film (subtracting out the effect of defects that occur in

close proximity to the grain boundary), and C_{ss} defines the steady-state concentration of defects in a layer during deposition. C_{ss} is specifically given as

$$C_{ss} = \frac{c_{0f}}{R}\frac{1}{\left(1 + \frac{l}{R\tau_s}\right)} \tag{4}$$

with $\frac{c_{0f}}{R}$ being the steady state concentration of defects, R is still defined as the growth rate, and τ_s the characteristic time for a defect to diffuse to the surface and be annihilated. To generate a steady state stress value for energetic deposition, Eqs. (1)–(3) are combined ($\sigma_{steadystate}^{sputtering} = \sigma_{growth} + \sigma_{gb}^{energetic} + \sigma_{bulk}^{energetic}$) to generate a total stress description below

$$\sigma_{steadystate}^{sputtering} = \left[\sigma_c + (\sigma_T - \sigma_C)e^{-\frac{\beta D}{RL}}\right] + A_0\left(\frac{l}{L}\right) + \left(1 - \frac{l}{L}\right)\frac{B_0}{\left(1 + \frac{l}{R\tau_s}\right)} \tag{5}$$

Note that $\sigma_0 C_{ss}$ is now replaced with a constant B_0 for ease of fitting to the experimental data. In this simplified form, the stress in the film is related to grain size, L, growth rate, R, and pressure (via the A_o and B_o terms).

While the individual effects of changing either the non-energetic or the energetic processing parameters are well documented in the literature, the combined effects and interplay between these two processes are not fully linked. Thus, the kinetic model here has the capability to potentially shed light on these processes by how the experimental data fit to behavior predicted by the balance of all the terms in Eq. (5). Nevertheless, the validity of the kinetic model needs to be confirmed through comparisons with experimental data to check for its consistency in fitting the correct stress-deposition trends.

Prior comparisons for electrodeposited Cu [25,32] and Ni [7,25] have shown good agreement using the non-energetic growth portions of the model, i.e. Eq. (1). As already mentioned above, for low mobility energetic growth, good agreement has also been shown in sputtered Mo [27], but was rather limited in parametric space. In particular, low deposition rates were not explored in this work, we expand the experimental parametric experimental space and use Cu, a high mobility adatom, under energetic deposition. To date, there have not been any holistic processing conditions for these types of films to be compared to the kinetic model. In addition, Cu is an excellent case study because it is technically important to several thin film technologies as electrical connectors, can be produced with an ultrafine grained microstructure at large scale for nanocrystalline applications [33] and has a database from electrodeposition from which we can compare to in the framework of the kinetic model above.

3. Material and methods

The Cu films for the stress measurements were deposited using balanced magnetron sputtering in an AJA ATC-1500 stainless-steel chamber. To achieve the desired deposition rate for the specific conditions used in this study, the films were deposited from either a single 2″ diameter Cu target or co-sputtered using two to four 2″ diameter Cu targets all having a purity of > 99.95%. All of the films were deposited at ambient temperature onto a Si [100] substrate that had a thermally grown 100 nm surface oxide. The effect of substrate heating from the operation of multiple cathodes was noted to be negligible due to the limited deposition time for the films. Additionally, this is also contributed to a moderately large substrate-to to cathode distance of 16 cm. The base pressure prior to deposition was $< 1.33 \times 10^{-5}$ Pa, where ultrahigh purity Ar was flowed at 15 standard cubic centimeters per minute to 0.267 Pa for the sputtering working gas. An initial 50 nm Cu "seed" layer was deposited at a rate of 0.12 nm/s to establish a uniform starting grain morphology and size distribution for every subsequent different deposition condition. Upon completion of the seed layer from those growth conditions, the deposition rate and pressure was immediately changed to one of the following conditions: 0.267 Pa and 0.012 nm/s, 0.12 nm/s, 1.2 nm/s and 2.4 nm/s deposition rates; 1.333 Pa and 0.012 nm/s, 0.12 nm/s and 1.2 nm/s deposition rates; and 2.667 Pa with deposition rates of 0.012 nm/s, 0.12 nm/s and 1 nm/s. This latter growth will be referred to as the "film" layer. The specific thicknesses of the film layer were varied between each of the aforementioned deposition conditions depending on the observed changes in the films' microstructure with increased layer thickness. Attention to this particular grain size was done to mitigate significant microstructural changes from occurring under the new deposition conditions, where grain growth or voiding can become more prevalent and contribute a microstructural variation effect to the stress response. Under such conditions, deciphering processing dependent and microstructural dependent contributions to the stress would be difficult. The growth rates at each pressure condition were determined using a quartz crystal microbalance calibrated by comparing measurements with small angle X-ray reflectivity [34] using an X'Pert Philips X-ray diffractometer (XRD) operated with a Cu K_α source at 45 kV and 40 mA.

All the intrinsic stress measurements were collected in-situ during film growth using a K-Space Associates® multibeam optical sensor system (MOS). This unit measures the change in the radius of curvature of the substrate using a reflected laser beam that is passed through an etalon creating an array of spots that reflect off of the substrate and are collected on a charge coupled device camera [35]. The relative displacement between the laser spots in the array is measured and then used to calculate the average stress in the film via the Stoney equation,

$$\sigma t_f = \frac{M_s t_s^2 \cos\alpha}{12L}\frac{\delta d}{d} \tag{6}$$

where M_s is the biaxial modulus of the substrate, t_s and t_f are the thickness of the substrate (250 μm) and thin film respectively, α is the angle of incidence of the laser beam (2°), L is the substrate detector optic length (88 cm) and $\frac{\delta d}{d}$ is the is the differential laser spot spacing on the detector [36]. The product σt_f which is proportional to the measured curvature is referred to as the stress-thickness. The use of relative displacement in the array of laser spots makes the measurement insensitive to the vibration generated by the vacuum pumping system. An average error in the stress measurements for each of the specific deposition conditions was determined by looking at the variation in the seed layer measurements, which offered a reasonable estimate considering multiple, identical deposition condition stress measurements were made through the course of the entire study.

Samples for microstructural characterization were prepared by a lift-out technique described elsewhere [37] using a FEI Quanta 200 Dual-Beam SEM-FIB. The transmission electron microscopy (TEM) samples were prepared in cross section and analyzed using a FEI Tecnai G^2 Supertwin TEM. In addition, orientation mapping of the samples was performed with the Nanomegas ASTAR system in the TEM using a precession angle of 2° and a step size of 3 nm to give grain size measurements [38]. Chemical analysis to measure oxygen content in the films was also performed using atom probe tomography (APT) with these samples also prepared using a lift-out technique [39]. Oxygen has been reported to effect the stress responses in Cu film [40]. The APT specimens were field evaporated in a Cameca local electrode atom probe (LEAP) 5000 XS using a laser mode with a pulse energy of 50 pJ, a set-point temperature of 40 K, a detection rate of 0.5% and a pulse frequency of 333 kHz. Analysis of the atom probe data was performed in IVAS 3.8.

4. Results & discussion

The in-situ stress measurements for all the deposition conditions are displayed in Fig. 1. The first 50 nm of growth corresponds to the seed layer to control the subsequent grain size which will be further elaborated upon below. Each of these 'seed' stress thickness product vs thickness curves is consistent with each other demonstrating good

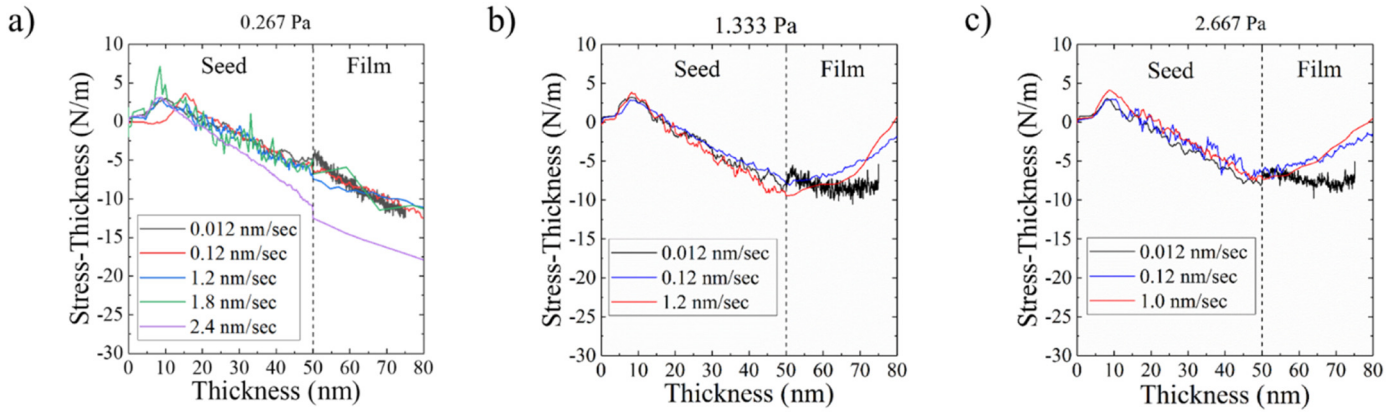

Fig. 1. Stress thickness plots for films deposited at (a) 0.266 Pa (b) 1.33 Pa and (c) 2.66 Pa. Color available online.

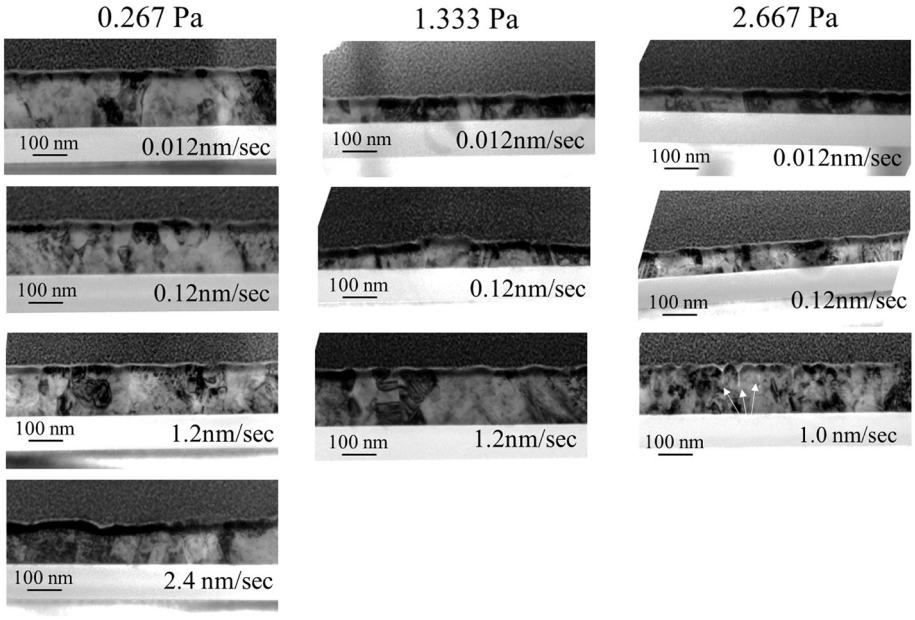

Fig. 2. Bright field cross sectional TEM images of the films grown on the seed layer.

reproducibility. After the seed deposition, the growth conditions were then changed to explore the effects of process on stress evolution. During this changeover, a small (~1–3 nm) transient region developed at the start of the film growth, which could be expected considering the extreme variations in process variables (for some cases) the film underwent from the seed growth conditions. The curves after this transient were observed to be relatively linear for the length of the subsequent deposition for many of the conditions studied. This linear slope infers that the film experienced little to no grain growth or microstructural change. This was confirmed by cross-sectional TEM images in Fig. 2. However, we do note, that at the higher-pressures, particularly in the thicker thicknesses, some curvature in the stress thickness plots do appear. This is believed to be associated to density changes within the film created by voiding in the microstructure. This phenomenon is commonly observed in high-pressure deposition conditions [41] and/or a dependence of the growth stress on the grain size [6]. We believe it is likely a voiding issue, evident by the onset of pores within the columnar grain boundaries near the surface of these films. This is shown by the white arrows for the 2.667 Pa 1.2 nm/s film's cross section in Fig. 2. For this reason, we analyzed the stress over film thicknesses of 25 to 50 nm depending on the magnitude of this effect. Within this thickness range, a linear growth response, after the initial transient behavior, was observed and provided the consistent data between the process variables for comparison to the kinetic model.

Besides identification of potential defects in the microstructure, Fig. 2 also confirmed the continuous microstructure between the seed and film layers. In these images, it is difficult, if not impossible, to distinguish the seed layer from the film suggesting that the corresponding film did indeed grow epitaxially on the grains of the seed layer thereby maintaining the initial microstructural control we required. Note that the dark region observed at the top of the films in some samples is an artifact related to Ga damage due to the sample preparation. To generate a more quantitative picture of the microstructure, orientation maps were collected using precession electron diffraction (PED) with the grain sizes displayed in Table 1. The average grain size across all the samples was 22.5 ± 4 nm with a range that spanned 16.7–29.3 nm. In our initial efforts, if we did not use this seed layer, we observed grain size variations over two orders of magnitude between the processing conditions. Besides the normal experimental distributions in grain sizes, the limited cross sectional sampling area used (typically 150 nm × 2 μm) would also contribute to the small size variations noted. For example, if the sampling area had a single, large grain in it, this would have a disproportional effect on the final size distribution. Regardless of these issues – expected experiential variation and sampling size – the data does demonstrate a reasonably good control of the film microstructure. As will be shown in the latter fitting

Table 1
Average grain size measurements (in cross-section) obtained from PED.

Grain size (nm)					
Deposition pressure (Pa)	Deposition rate (nm/s)				
	0.012	0.12	1.0	1.2	2.4
0.267	18.5 ± 20.2	23.2 ± 16.1	x	24.4 ± 17.6	29.4 ± 29.7
1.333	16.7 ± 14.0	20.6 ± 12.9	x	25.3 ± 22.1	x
2.667	24.0 ± 17.6	24.9 ± 17.8	18.0 ± 9.8	x	x

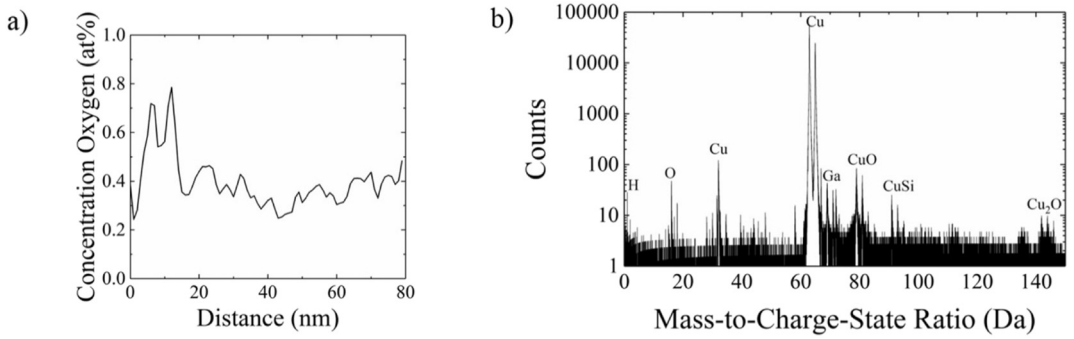

Fig. 3. (a) Concentration profile showing little to no variation in oxygen content through film thickness. (b) Mass spectrum form APT, note the love level of oxygen.

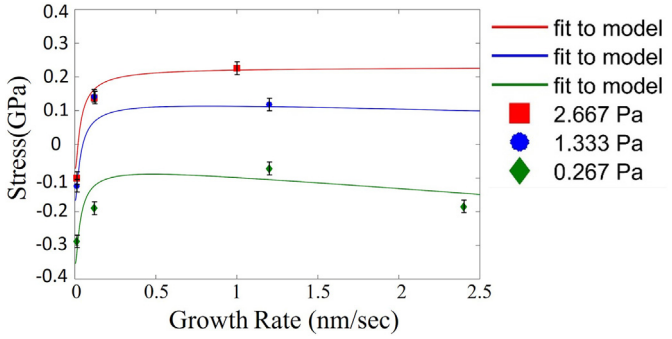

Fig. 4. Kinetic model fitting curves (solid lines) overlaid on stress verses growth rate measurements of Cu. Color available online.

to the kinetic model, a lack of any clear trend with grain size associated with deposition rate and/or pressure was found furthering supporting that any grain size variation was not a significant factor on the stress response.

Besides grain size, oxygen can also influence Cu film stress [40]. To ensure that the films did not have this potential effect, we performed APT at the highest deposition pressure where the potential for oxygen contamination would be the maximum since the highest deposition pressure would be from the reduced pumping speed in the deposition chamber as the gate value was nearly closed off. Fig. 3 is the time-of-flight mass spectrum from the field evaporation as well as the concentration profile as a function of film depth, which would quantify potential oxygen migration through the film as it grew. The results revealed that the oxygen content was ~0.3 at.% with minimal oxygen variation through the film depth. This low oxygen content is contributed either from the target itself, the background gas in the chamber, and/or during the sample transfer between the deposition to the LEAP chamber (< 24 h). Its low value provides confidence that oxygen-based effects are negligible in the forthcoming stress results discussion.

Returning to Fig. 1(a), the stress-thickness evolution at the different deposition rates for the pressure of 0.267 Pa are plotted. As the deposition rate increased from 0.012 nm/s to 1.2 nm/s, the steady state stress (which is the slope of the curve) was observed to decrease (or become less compressive). With a further increase in the rate to 1.8 nm/s and then 2.4 nm/s, the steady-state compressive stress then increased (or became more compressive). This initial decrease in the steady state stress is consistent with prior work for non-energetic depositions, where lower deposition rates are associated with larger compressive stresses [22,42]. The change in the compressive stress at the higher deposition rates is believed to be associated with the trapping of defects in the bulk of the film [43–46]. Through our comprehensive span of deposition rates, within one study, both effects are captured. Upon looking at the higher deposition pressures of 1.333 Pa and 2.667 Pa, Fig. 1(b) and (c) respectively, the slope of the stress response is observed to become more tensile as the deposition rate is increased and we no longer see this transition in slope seen in the lower pressure conditions.

The steady-state stress data obtained from the slope of the stress-thickness, Fig. 1, are plotted against the growth rate at the different measured pressures in Fig. 4. Several trends can be noted in this data representation. For each growth rate, the stress is more compressive when the pressure is lower. For the lowest growth rates, the stress is more compressive than at high growth rates for all pressures. However, there is a different behavior for the stress at high growth rates depending on the pressure. For the low-pressure regime, the stress appears to become more compressive at the highest growth rates. At high pressure, the stress appears to retain the same tensile value when the growth rate is increased. Experimental limitations made it impossible to measure the same range of growth rates for all the pressures, so growth rates > 1.2 nm/s could not be measured at high pressure. However, previous studies of non-energetic deposition of Cu [25] also show that the tensile stress is retained at high growth rates.

The dependence of the steady-state stress in Fig. 4 can now be fitted to the kinetic model given in Eq. (5), shown as solid lines. Note that the experimental data points have associated error bars that originate from the slope obtained from performing duplicate measurements at each deposition condition. The similar responses provide confidence in the reproducibility of the stress states under the specific deposition condition. The optimum values for the parameters were obtained by using a non-linear least-squares fitting routine that minimized the residual between the model and the measurements. Because of the large number of potential fitting parameters, we constrained A_o, B_o and l to have a

Table 2
Values obtained when applying the non-linear least squares fitting of the stress data to the kinetic model.

Pressure (Pa)	σ_C (GPa)	σ_T (GPa) at L = 22.5 nm	βD (nm^2/s)	D_i (nm^2/s)	P_0 (Pa)	A_0 (GPa)	B_0 (GPa)	l (nm)
0.267	−0.0707	0.23	0.67	5503.14	2.81	−3.82	−131.19	1.67
1.333	−0.0707	0.23	0.67	5503.14	2.81	−2.22	−76.24	0.97
2.667	−0.0707	0.23	0.67	5503.14	2.81	−0.22	−7.475	0.10

linear dependence on the pressure below a threshold value of P_o with further details of this fitting discussed in reference [27]. This constraint makes the magnitude of these parameters increase with particle energy. Enforcing a linear dependence on pressure reduces the number of free parameters from thirteen to eight. The constrained parameters were then optimized over the entire data set to produce physically reasonable values that can then be used to compare the calculations between the different data sets. The resulting fitting parameters are tabulated in Table 2.

Comparing the experimental data and fitting results from the kinetic model, Fig. 4, the model is capturing the growth rate and pressure dependence trends on the stress evolution in the energetically deposited, high mobility system. To understand these fitting parameters produced by the model, comparisons between these values and different elemental systems and deposition techniques were undertaken. Nonetheless, one should exhibit measured caution on strict comparisons between the absolute fitting parameter values. Since they are fitted from experimental data, there will be some uncertainty from those measurements. If the uncertainty were only from experimental error, then statistical analysis would be sufficient to determine the fitting parameter uncertainty. However, simplifying assumptions were required in the model and these assumptions would also contribute to differences from the data. Such systematic errors would then indicate that differences between the fit and the experimental data are not strictly related to statistical experimental error. Thus, the fitting parameters are 'best values' but do not have their own errors reported, as they would be convoluted between the experimental and modeling assumptions' uncertainties. Rather these fitting parameters provide semi-quantitative information that aid in the exploration of trends and help provide insights into the stress generating contributions from different physical mechanisms that may otherwise be unavailable to assess.

To begin this comparison, we will relate the experimental data reported for the low mobility Mo films provided in the supplementary information [27] to our high mobility Cu films. While the Mo data was obtained over a much narrower pressure range (0.11–0.43 Pa) and growth rates (0.05–0.3 nm/s) than the Cu films studied here, it does contain some overlap in processing conditions. In the highest deposition pressure regime for Mo (0.43 Pa), the steady-state stress was tensile and exhibited little to no dependence on growth rate. In contrast, for Cu at the highest deposition pressure (2.66 Pa), the film exhibited a much stronger rate dependence, becoming more tensile with increasing deposition rate. At the lowest deposition rate for the high pressure Cu, a compressive stress was observed which was not experimentally reported in the Mo study. Considering that the Cu was deposited at a much higher pressure than Mo, this difference in behavior is striking because one might assume at higher pressures, with the reduction of energetic contributions, the stress would remain tensile over the entirety of growth conditions. The difference in the behavior for Cu can be attributed to the effect of the non-energetic growth stresses in Eq. (5). For the higher atomic mobility Cu, the growth stress is predicted to become compressive at low growth rates. For the low mobility Mo, the reported growth stress remains tensile over the range of growth rates measured. In terms of the kinetic model, this behavior is predicted by the dependence on the kinetic parameter βD. For large values of $\beta D/R$ (as in Cu), the stress is predicted to become compressive while for low values (as in Mo), it remains tensile.

At low pressures, the energetic effects of the incoming species become greater than at high pressures. For this reason, at each growth rate, the stress becomes more compressive as the pressure is lowered. Furthermore, for the experimental data in the Mo study at low pressure, the compressive stress becomes even more compressive as the deposition rate increases. This same behavior is observed in the Cu system in the higher deposition rate regime when increasing the deposition rate from 1.2 nm/s to 2.4 nm/s. In these cases, the stress effect due to the impact of energetic particle becomes larger when the flux of energetic particles is larger. The fact that the stress becomes more compressive at higher growth rates suggests that the energetic effects are larger than the growth effects. Conversely, at the lowest Cu deposition rate, a stress turnaround is observed and the compressive stress becomes more compressive at low growth rates. This again can be attributed to the effect of the growth stress being larger than that of the energetic particle stress at the low growth rates. This turnaround behavior fits well to the kinetic model for the Cu system, Fig. 4's 0.267 Pa fit. In the case of Mo, similar behavior is predicted for the lower growth rates, but it was not observed because the experimental data was not acquired at a sufficiently low growth rate. By going to a higher mobility material, like Cu, we have been able to observe this crossover between the energetic and growth stress behavior as predicted by the model.

At high growth rates and low deposition pressures, the arrival energy of the sputtered atoms would be high. In this condition, the stress would be predicted to become ever more compressive because the high arrival energies provide a mechanism for more defects to be incorporated into the films. This mechanism is predicted by the model and was observed in both this work and the Mo study, with the slope of the stress verses growth rate (in the high growth rate regime) being greater for Mo. This would indicate that more defects are being incorporated into the Mo film because Mo has lower diffusivity than Cu which would enable it to trap these defects. In the kinetic model, this defect incorporation is reflected in the B_0 term. Considering the cases where the Mo and Cu pressures are similar (0.24 Pa verses 0.267 Pa, respectively), we have used the same fitting routine to both datasets, with the Mo data fits provided as a supplement to this paper. The B_0 for Mo was approximately −501 GPa and for Cu it was −131 GPa. Though there can be some uncertainty in the absolute values used, the nearly 3.5× difference does demonstrate a significant effect where one can reasonably infer that indeed the defect incorporation is higher in Mo than that of Cu or that a defect in Cu contributes a small contribution to the stress than that in Mo. The ability to use the kinetic model to begin to semi-quantitatively ascertain such contributions provides potential toolset to compare stress behavior mechanisms and contributions across systems.

While there are many differences that can exist between sputter-deposition and electrodeposition, comparing the growth stresses, which are believed to be independent of the energetic contributions of sputtering, allows for another opportunity to compare the stress influences between the two techniques. When looking at the growth contributions of σ_c and σ_T in Eq. (1), the sputter-deposited Cu was approximately −70 MPa and 230 MPa respectively whereas electrodeposited Cu is approximately −19.9 MPa [25] and 380 MPa [25] respectively for the same grain size. We once again recognize that care should be taken in any comparison of the absolute parameters, but the values are relatively

comparable (and within the same order of magnitude) between the two techniques which adds confidence in the kinetic model's ability to extract individual contributions to the stress in the sputtered deposition conditions. While further studies in more materials systems are needed to further elucidate a more thorough understanding of these observations, it does suggest that the intrinsic elemental, atomic mobility behavior does indeed influence stress effects. The good agreement of the kinetic model with this data, along with a prior study [27], indicates that the kinetic model has potential for understanding the contributions of different non-energetic and energetic growth processes to the stress evolution of thin films.

5. Summary

This work has examined the growth rate and pressure dependence on the intrinsic stress for sputter deposited Cu, a high mobility metal film. To mitigate the effect of microstructure, i.e. grain growth and size, to the stress evolution, a 50 nm Cu seed layer was deposited for all films under identical deposition conditions. It was found that by establishing a seed layer it was sufficient in keeping the subsequent Cu films morphology, from rates of 0.012 nm/s to 2.4 nm/s and pressures between 0.267 Pa to 2.667 Pa, relatively similar up to 50 nm. The linear steady-state growth enabled the effect of processing changes to be ascertained. It was found that the intrinsic stress exhibited a rate dependent behavior with different trends emerging for high and low deposition pressures, which where fitted to a kinetic model that contains contributions from growth and energetic stress generation mechanisms. At high deposition pressures, the stress became more tensile as the growth rate increased. In the low deposition pressure regime, the stress became more tensile with increases in deposition rate until a critical cross-over point where further increases in deposition rate resulted in the stress becoming more compressive. This cross-over has been explained in terms of the energetic contributions to the stress. The ability to observe the crossover by Cu is contributed to its high intrinsic mobility; in previous work in Mo, a low mobility film, this crossover behavior was not observed. Through the use of the kinetic model, the fitting parameters and corresponding stress contributions were extracted and compared to other films and deposition techniques. Though caution should be used in comparing absolute values between these findings and prior reported values, as various uncertainties exist, the kinetic model revealed the correct trends in predicting energetic trapping of defects between low and high mobility films as well as similar growth stress values, which are independent of energetic contributions, between sputtering and electrodeposition. The kinetic model, with the experimental data here, appears to be a promising description in revealing and understanding the different contributions of intrinsic thin film stress.

Acknowledgments

The authors TK and GBT gratefully acknowledge the Army Research Office, Grant No. W911NF1310436, Dr. Michael Bakas, program manager. The work of EC and ZR was supported by the NSF under contract DMR-1602491. The UA Central Analytical Facility is recognized for additional assistance and access to the microscopes used in this research. Finally, the authors thank Thomas Koenig for his assistance.

Appendix A. Supplementary data

Supplementary data to this article can be found online at https://doi.org/10.1016/j.surfcoat.2018.10.059.

References

[1] R. Koch, The intrinsic stress of polycrystalline and epitaxial thin metal films, J. Phys. Condens. Matter 6 (1994) 9519–9550, https://doi.org/10.1088/0953-8984/6/45/005.
[2] T.M. Shaw, Z. Suo, M. Huang, E. Liniger, R.B. Laibowitz, J.D. Baniecki, The effect of stress on the dielectric properties of barium strontium titanate thin films, Appl. Phys. Lett. 75 (1999) 2129–2131, https://doi.org/10.1063/1.124939.
[3] M.-W. Moon, J.-W. Chung, K.-R. Lee, K.H. Oh, R. Wang, A.G. Evans, An experimental study of the influence of imperfections on the buckling of compressed thin films, Acta Mater. 50 (2002) 1219–1227, https://doi.org/10.1016/S1359-6454(01)00423-2.
[4] V.B. Shenoy, A.F. Schwartzman, L.B. Freund, Crack patterns in brittle thin films, Int. J. Fract. 103 (2000) 1–17, https://doi.org/10.1023/A:1007673320058.
[5] G. Gore, On the properties of electro-deposited antimony, Philos. Trans. R. Soc. Lond. 148 (1858) 185–197.
[6] H.Z. Yu, C.V. Thompson, Grain growth and complex stress evolution during Volmer–Weber growth of polycrystalline thin films, Acta Mater. 67 (2014) 189–198, https://doi.org/10.1016/j.actamat.2013.12.031.
[7] E. Chason, A.M. Engwall, Relating residual stress to thin film growth processes via a kinetic model and real-time experiments, Thin Solid Films 596 (2015) 2–7, https://doi.org/10.1016/j.tsf.2015.06.061.
[8] A. Bhandari, B.W. Sheldon, S.J. Hearne, Competition between tensile and compressive stress creation during constrained thin film island coalescence, J. Appl. Phys. 101 (2007) 033528, , https://doi.org/10.1063/1.2432376.
[9] A.A. Navid, E. Chason, A.M. Hodge, Evaluation of stress during and after sputter deposition of Cu and Ta films, Surf. Coat. Technol. 205 (2010) 2355–2361, https://doi.org/10.1016/j.surfcoat.2010.09.020.
[10] R. Abermann, Measurements of the intrinsic stress in thin metal films, Vacuum 41 (1990) 1279–1282, https://doi.org/10.1016/0042-207X(90)93933-A.
[11] E. Bauer, Phänomenologische Theorie der Kristallabscheidung an Oberflächen. I, Z. Krist. 110 (1958) 372–394, https://doi.org/10.1524/zkri.1958.110.1-6.372.
[12] R.C. Cammarata, T.M. Trimble, D.J. Srolovitz, Surface stress model for intrinsic stresses in thin films, J. Mater. Res. 15 (2000) 2468–2474, https://doi.org/10.1557/JMR.2000.0354.
[13] R.W. Hoffman, Stresses in thin films: the relevance of grain boundaries and impurities, Thin Solid Films 34 (1976) 185–190, https://doi.org/10.1016/0040-6090(76)90453-3.
[14] W.D. Nix, B.M. Clemens, Crystallite coalescence: a mechanism for intrinsic tensile stresses in thin films, J. Mater. Res. 14 (1999) 3467–3473, https://doi.org/10.1557/JMR.1999.0468.
[15] R. Koch, D. Hu, A.K. Das, Compressive stress in polycrystalline Volmer–Weber films, Phys. Rev. Lett. 94 (2005) 146101, , https://doi.org/10.1103/PhysRevLett.94.146101.
[16] C. Friesen, S.C. Seel, C.V. Thompson, Reversible stress changes at all stages of Volmer–Weber film growth, J. Appl. Phys. 95 (2004) 1011–1020, https://doi.org/10.1063/1.1637728.
[17] F. Spaepen, Interfaces and stresses in thin films, Acta Mater. 48 (2000) 31–42, https://doi.org/10.1016/S1359-6454(99)00286-4.
[18] E. Chason, B.W. Sheldon, L.B. Freund, J.A. Floro, S.J. Hearne, Origin of compressive residual stress in polycrystalline thin films, Phys. Rev. Lett. 88 (2002) 156103, , https://doi.org/10.1103/PhysRevLett.88.156103.
[19] D. Magnfält, A. Fillon, R.D. Boyd, U. Helmersson, K. Sarakinos, G. Abadias, Compressive intrinsic stress originates in the grain boundaries of dense refractory polycrystalline thin films, J. Appl. Phys. 119 (2016) 055305, , https://doi.org/10.1063/1.4941271.
[20] G. Carter, Peening in ion-assisted thin-film deposition: a generalized model, J. Phys. D. Appl. Phys. 27 (1994) 1046, https://doi.org/10.1088/0022-3727/27/5/024.
[21] G. Thurner, R. Abermann, Internal stress and structure of ultrahigh vacuum evaporated chromium and iron films and their dependence on substrate temperature and oxygen partial pressure during deposition, Thin Solid Films 192 (1990) 277–285, https://doi.org/10.1016/0040-6090(90)90072-L.
[22] A.L.D. Vecchio, F. Spaepen, The effect of deposition rate on the intrinsic stress in copper and silver thin films, J. Appl. Phys. 101 (2007) 063518, , https://doi.org/10.1063/1.2712150.
[23] M. Pletea, W. Brückner, H. Wendrock, R. Kaltofen, Stress evolution during and after sputter deposition of Cu thin films onto Si (100) substrates under various sputtering pressures, J. Appl. Phys. 97 (2005) 054908, , https://doi.org/10.1063/1.1858062.
[24] A. Fillon, G. Abadias, A. Michel, C. Jaouen, Stress and microstructure evolution during growth of magnetron-sputtered low-mobility metal films: influence of the nucleation conditions, Thin Solid Films 519 (2010) 1655–1661, https://doi.org/10.1016/j.tsf.2010.07.091.
[25] A.M. Engwall, Z. Rao, E. Chason, Origins of residual stress in thin films: interaction between microstructure and growth kinetics, Mater. Des. 110 (2016) 616–623, https://doi.org/10.1016/j.matdes.2016.07.089.
[26] E. Chason, J.W. Shin, S.J. Hearne, L.B. Freund, Kinetic model for dependence of thin film stress on growth rate, temperature, and microstructure, J. Appl. Phys. 111 (2012) 083520, , https://doi.org/10.1063/1.4704683.
[27] E. Chason, M. Karlson, J.J. Colin, D. Magnfält, K. Sarakinos, G. Abadias, A kinetic model for stress generation in thin films grown from energetic vapor fluxes, J. Appl. Phys. 119 (2016) 145307, , https://doi.org/10.1063/1.4946039.
[28] L.B. Freund, E. Chason, Model for stress generated upon contact of neighboring islands on the surface of a substrate, J. Appl. Phys. 89 (2001) 4866–4873, https://doi.org/10.1063/1.1359437.
[29] C. Friesen, C.V. Thompson, Reversible stress relaxation during precoalescence interruptions of Volmer–Weber thin film growth, Phys. Rev. Lett. 89 (2002) 126103, , https://doi.org/10.1103/PhysRevLett.89.126103.
[30] A.M. Engwall, Z. Rao, E. Chason, Residual stress in electrodeposited Cu thin films: understanding the combined effects of growth rate and grain size, J. Electrochem. Soc. 164 (2017) D828–D834, https://doi.org/10.1149/2.0921713jes.

[31] D. Magnfalt, G. Abadias, K. Sarakinos, Atom insertion into grain boundaries and stress generation in physically vapor deposited films, Appl. Phys. Lett. 103 (5) (2013), http://aip.scitation.org/doi/full/10.1063/1.4817669 , Accessed date: 6 June 2017.
[32] E. Chason, A. Engwall, F. Pei, M. Lafouresse, U. Bertocci, G. Stafford, J.A. Murphy, C. Lenihan, D.N. Buckley, Understanding residual stress in electrodeposited Cu thin films, J. Electrochem. Soc. 160 (2013) D3285–D3289, https://doi.org/10.1149/2.048312jes.
[33] A.M. Hodge, Y.M. Wang, T.W. Barbee, Large-scale production of nano-twinned, ultrafine-grained copper, Mater. Sci. Eng. A 429 (2006) 272–276, https://doi.org/10.1016/j.msea.2006.05.109.
[34] Y. Sasanuma, M. Uchida, K. Okada, K. Yamamoto, Y. Kitano, A. Ishitani, Characterization of long-periodic layered structures by X-ray diffraction IV: small angle X-ray diffraction from a superlattice with non-ideal interfaces, Thin Solid Films 203 (1991) 113–120, https://doi.org/10.1016/0040-6090(91)90522-Y.
[35] C. Taylor, D. Bartlett, E. Chason, J. Floro, The Industrial Physicists, 4 (1998), p. 25.
[36] G.G. Stoney, The tension of metallic films deposited by electrolysis, Proc. R. Soc. A Math. Phys. Eng. Sci. 82 (1909) 172–175, https://doi.org/10.1098/rspa.1909.0021.
[37] L.A. Giannuzzi, F.A. Stevie, A review of focused ion beam milling techniques for TEM specimen preparation, Micron 30 (1999) 197–204, https://doi.org/10.1016/S0968-4328(99)00005-0.
[38] E.F. Rauch, M. Véron, J. Portillo, D. Bultreys, Y. Maniette, S. Nicolopoulos, Automatic crystal orientation and phase mapping in TEM by precession diffraction, Microsc. Anal. U. K. 128 (2008) S5–S8.
[39] K. Thompson, D. Lawrence, D.J. Larson, J.D. Olson, T.F. Kelly, B. Gorman, In situ site-specific specimen preparation for atom probe tomography, Ultramicroscopy 107 (2007) 131–139, https://doi.org/10.1016/j.ultramic.2006.06.008.
[40] R. Abermann, R. Koch, In situ study of thin film growth by internal stress measurement under ultrahigh vacuum conditions: silver and copper under the influence of oxygen, Thin Solid Films 142 (1986) 65–76, https://doi.org/10.1016/0040-6090(86)90303-2.
[41] J.A. Thornton, High rate thick film growth, Annu. Rev. Mater. Sci. 7 (1977) 239–260, https://doi.org/10.1146/annurev.ms.07.080177.001323.
[42] A.L. Shull, F. Spaepen, Measurements of stress during vapor deposition of copper and silver thin films and multilayers, J. Appl. Phys. 80 (1996) 6243–6256, https://doi.org/10.1063/1.363701.
[43] C.A. Davis, A simple model for the formation of compressive stress in thin films by ion bombardment, Thin Solid Films 226 (1993) 30–34, https://doi.org/10.1016/0040-6090(93)90201-Y.
[44] H. Windischmann, An intrinsic stress scaling law for polycrystalline thin films prepared by ion beam sputtering, J. Appl. Phys. 62 (1987) 1800.
[45] F.M. D'Heurle, J.M.E. Harper, Note on the origin of intrinsic stresses in films deposited via evaporation and sputtering, Thin Solid Films 171 (1989) 81–92, https://doi.org/10.1016/0040-6090(89)90035-7.
[46] F. Cermin, G. Abadias, T. Minea, C. Furgeaud, F. Brisset, D. Solas, D. Lindin, Benefits of energetic ion bombardment for tailoring stress and microstructural evolution during growth of Cu thin films, Acta Mater. 141 (2017) 120–130.